CellPress
PARTNER JOURNAL

Molecular Plant
Research Article

Stripe Rust Effector PstGSRE1 Disrupts Nuclear Localization of ROS-Promoting Transcription Factor TaLOL2 to Defeat ROS-Induced Defense in Wheat

Tuo Qi[1,3], Jia Guo[1,3], Peng Liu[1], Fuxin He[1], Cuiping Wan[1], Md Ashraful Islam[1], Brett M. Tyler[2], Zhensheng Kang[1,*] and Jun Guo[1,*]

[1]State Key Laboratory of Crop Stress Biology for Arid Areas, College of Plant Protection, Northwest A&F University, Yangling 712100, Shaanxi, P. R. China

[2]Center for Genome Research and Biocomputing, Oregon State University, Corvallis, OR, USA

[3]These authors contributed equally to this article.

***Correspondence: Zhensheng Kang (kangzs@nwsuaf.edu.cn), Jun Guo (guojunwgq@nwsuaf.edu.cn)**

https://doi.org/10.1016/j.molp.2019.09.010

ABSTRACT

***Puccinia striiformis* f. sp. *tritici* (*Pst*), a biotrophic plant pathogen, secretes numerous effectors to modulate host defense systems. Understanding the molecular mechanisms by which *Pst* effectors regulate wheat immunity is of great importance for the development of novel strategies for durable control of stripe rust. In this study, we identified a glycine-serine-rich effector gene, *PstGSRE1*, which is highly induced during early infection. Transgenic expression of *PstGSRE1* RNAi constructs in wheat significantly reduced virulence of *Pst* and increased H_2O_2 accumulation in wheat. PstGSRE1 was shown to target the reactive oxygen species (ROS)-associated transcription factor TaLOL2, a positive regulator of wheat immunity. PstGSRE1 disrupted nuclear localization of TaLOL2 and suppressed ROS-mediated cell death induced by TaLOL2, thus compromising host immunity. This work reveals a previously unrecognized strategy whereby rust fungi exploit the PstGSRE1 effector to defeat ROS-associated plant defense by modulating the subcellular compartment of a host immune regulator and facilitate pathogen infection.**

Key words: host-induced gene silencing, effector, glycine-serine-rich, transcription factor, *Puccinia striiformis* f. sp. *tritici*, reactive oxygen species

Qi T., Guo J., Liu P., He F., Wan C., Islam M.A., Tyler B.M., Kang Z., and Guo J. (2019). Stripe Rust Effector PstGSRE1 Disrupts Nuclear Localization of ROS-Promoting Transcription Factor TaLOL2 to Defeat ROS-Induced Defense in Wheat. Mol. Plant. **12**, 1624–1638.

INTRODUCTION

Plants have evolved two overlapping defense responses against most pathogenic microbes. These defense responses include the deposition of callose, the induction of reactive oxygen species (ROS), the reinforcement of plant cell-wall components, and the expression of defense-related genes (Jones and Dangl, 2006). One mechanism by which these defenses are activated is through the perception of pathogen-associated molecular patterns (PAMPs) by pattern recognition receptors, which produce a response known as a PAMP-triggered immunity (PTI) (Dangl and Jones, 2001). To suppress PTI, pathogens deploy virulence proteins called effectors to modulate host defense responses. To combat effectors, plants have evolved resistance (R) proteins that recognize certain effectors, termed avirulence (AVR) effectors, and trigger a second, more rapid immune response, termed effector-triggered immunity (ETI). ETI is often associated with a localized hypersensitive response (HR) at the site of infection (Thomma et al., 2011). A massive and sustained oxidative burst is induced during ETI, and ROS appear to act as a key component of the defense system (Lamb and Dixon, 1997; Gupta et al., 2015). ROS mediate diverse plant defense responses through a variety of signaling pathways, including protein phosphorylation-induced signaling cascades and pathways involving chemical signals (e.g., nitric oxide), and plant hormones (e.g., salicylic acid) (Karpiński et al., 2013). Negative regulators such as LSD1, and positive regulators such as

Published by the Molecular Plant Shanghai Editorial Office in association with Cell Press, an imprint of Elsevier Inc., on behalf of CSPB and IPPE, SIBS, CAS.

PAD4 and EDS1, are essential for regulating ROS production (Rustérucci et al., 2001).

Rust fungi are obligate biotrophs that form specialized infection structures called haustoria. Haustoria function in nutrient uptake and also in the production and release of effectors (Garnica et al., 2014). Numerous effectors such as AvrM and AvrL567 from *Melampsora lini* (*Ml*) (Ellis et al., 2007), RTP1 from *Uromyces fabae* (*Uf*) (Kemen et al., 2005), and AvrSr50 and AvrSr35 from *Puccinia graminis* f. sp. *tritici* (*Pgt*) (Chen et al., 2017b; Salcedo et al., 2017), as well as PEC6, PSTha5a23, and PST02549 from *Pst*, have been confirmed to be related to virulence or avirulence of the pathogen (Cheng et al., 2016; Liu et al., 2016; Tang et al., 2018). Some effectors are able to influence host immunity (Jiang and Tyler, 2012; Lo et al., 2015). For example, *Phytophthora sojae* RxLR effectors PSR1 and PSR2 influence the RNA-silencing process (Ye and Ma, 2016) and PsAvr3c reprograms pre-mRNA splicing (Huang et al., 2017), indicating that these effectors interfere with immunity at the transcriptional or post-transcriptional level in the host. Effectors may also target important signaling or defense proteins in the host. The bacterial effector AvrPtoB, as well as PNPi from *Pst*, directly target NPR1, a key regulator in the salicylic acid signaling pathway (Wang et al., 2016; Chen et al., 2017a). Pathogenesis-related protein 1 (PR1), a sterol-binding defense protein (Gamir et al., 2017) that is a marker for salicylic acid-dependent responses, has been shown to interact with effector SsCP1 from *Sclerotinia sclerotiorum* (Yang et al., 2018). Moreover, effectors may abolish ROS-mediated plant immune responses. ROS scavenging proteins, such as peroxidases and catalases, are compromised by effectors (Dong et al., 2011; Hemetsberger et al., 2012; Zhang et al., 2015). Targeting key immune components with effectors has emerged as a common strategy employed by pathogens to promote pathogenicity (Torto-Alalibo et al., 2010; Dou and Zhou, 2012).

In several organisms, glycine- or serine-rich proteins have been shown to participate in RNA splicing, metabolism, and signal transduction (Golovkin and Reddy, 1998; Mangeon et al., 2010). Therefore, pathogen effectors with a high content of glycine or serine could potentially modify the host's metabolism or signal transduction. In *Magnaporthe oryzae*, the glycine-rich protein Rbf1 participates in the formation of the biotrophic interfacial complex (Nishimura et al., 2016). *M. oryzae DES1* encodes a serine-rich protein that is required for neutralizing host ROS and regulating counter-defenses against host resistance (Chi et al., 2009). PWLs make up another family of small, glycine-rich effector proteins that are present in the rice blast pathogen and function as avirulence proteins during infection of weeping love grass and finger millet (Zhang and Xu, 2014). *Podosphaera xanthii* effector PEC034, which contains a glycine-rich region, interferes with vesicle trafficking of host plant cells by mimicking a host ALIX protein (Martínez-Cruz et al., 2018). In addition, harpins, characterized as small, acidic, glycine-rich, and heat-stable proteins, are secreted through the type III secretion system (T3SS) to suppress basal defense mechanisms and trigger the HR in the host plant (Büttner and Bonas, 2003). In *Pst*, several effectors have been identified (e.g., PSTha5a23, PEC6) (Cheng et al., 2016; Liu et al., 2016). However, the mechanisms of these effectors, especially the glycine-rich or serine-rich effectors (GSREs), remain obscure, and further investigation is required.

Stripe rust is one of the most devastating diseases in wheat (*Triticum aestivum*) worldwide (Garnica et al., 2014). In this study, we identified a glycine-serine-rich effector protein in *Pst* (PstGSRE1), which suppresses programmed cell death (PCD) triggered by Bax and by the elicitor-like protein Pst322, and which performs a positive function in *Pst* virulence. A wheat LSD-1-Like zinc-finger protein (TaLOL2), which is closely associated with the ROS signaling pathway, was identified as a target of PstGSRE1. We showed that TaLOL2 is a positive regulator of wheat resistance and that PstGSRE1 disrupts host immunity and promotes disease by disrupting nuclear accumulation of TaLOL2, providing new insights into the molecular mechanisms underlying the interaction between wheat and *Pst*.

RESULTS

PstGSRE1 Suppresses Bax- and Pst322-Induced Cell Death

Previous studies have shown that small pathogen-secreted proteins enriched in serine or glycine may act as effectors (Chi et al., 2009; Zhang and Xu, 2014; Nishimura et al., 2016; Martínez-Cruz et al., 2018). To search for such effectors in *Pst*, we analyzed the frequency of serine and glycine residues in predicted small secreted proteins. Our criterion was a glycine/serine content at least 2-fold higher than that of total *ab initio* annotations in the genome of *Pst* race CYR32 (Zheng et al., 2013), which is one of the most virulent and predominant races in China. This screen identified four small secreted proteins (Supplemental Table 1). Among these candidates, we focused on PSTCYR32_24 327, which exhibited the highest content of serine and glycine (36.21%). Sequence analysis showed that *PSTCYR32_24 327* encodes a 290-amino-acid (aa) secreted protein, which is enriched in glycine (14.83%) and serine (21.38%) and does not contain any known functional domains except for a 17-aa signal peptide at its N terminus. Thus, PSTCYR32_24 327 was designated *Puccinia striiformis* Glycine-Serine-Rich Effector 1 (PstGSRE1). BLASTp analyses revealed that homologs of PstGSRE1 can only be found in rust fungi, including 34 in *Pst*, three in *Puccinia triticina* (*Pt*), four in *Pgt*, four in *Uf*, and seven in *Puccinia sorghi* (*Pso*) (Supplemental Table 2), indicating that GSREs constitute a large family within the rust fungi. A relatively high level of conservation was observed among GSRE proteins from wheat stripe, leaf, and stem rust pathogens (Supplemental Figure 1A). As shown in Supplemental Figure 1B, the most similar homologs from *Pgt*, *Pt*, *Pso*, and *Uf* are all enriched in glycine and serine, i.e., PTTG_01 799 (18.71% glycine, 19.35% serine), PGTG_04 810 (14.81%, 18.23%), UF_g16974 (18.15%, 18.15%), and PSO_KNZ51316.1 (18.71%, 19.35%).

To examine the localization of PstGSRE1 inside plant cells, we transiently expressed a PstGSRE1-GFP fusion protein in wheat protoplasts. GFP fluorescence was observed mainly in the cytoplasm and nucleus, similar to free GFP (Supplemental Figure 2A). Secretion of PstGSRE1 was verified using a genetic assay based on the requirement of invertase secretion for yeast growth on medium with sucrose or raffinose as the sole carbon source (Jacobs et al., 1997). pSUC2T7M13ORI-SP-*PstGSRE1* was transferred into the yeast *SUC2*-minus

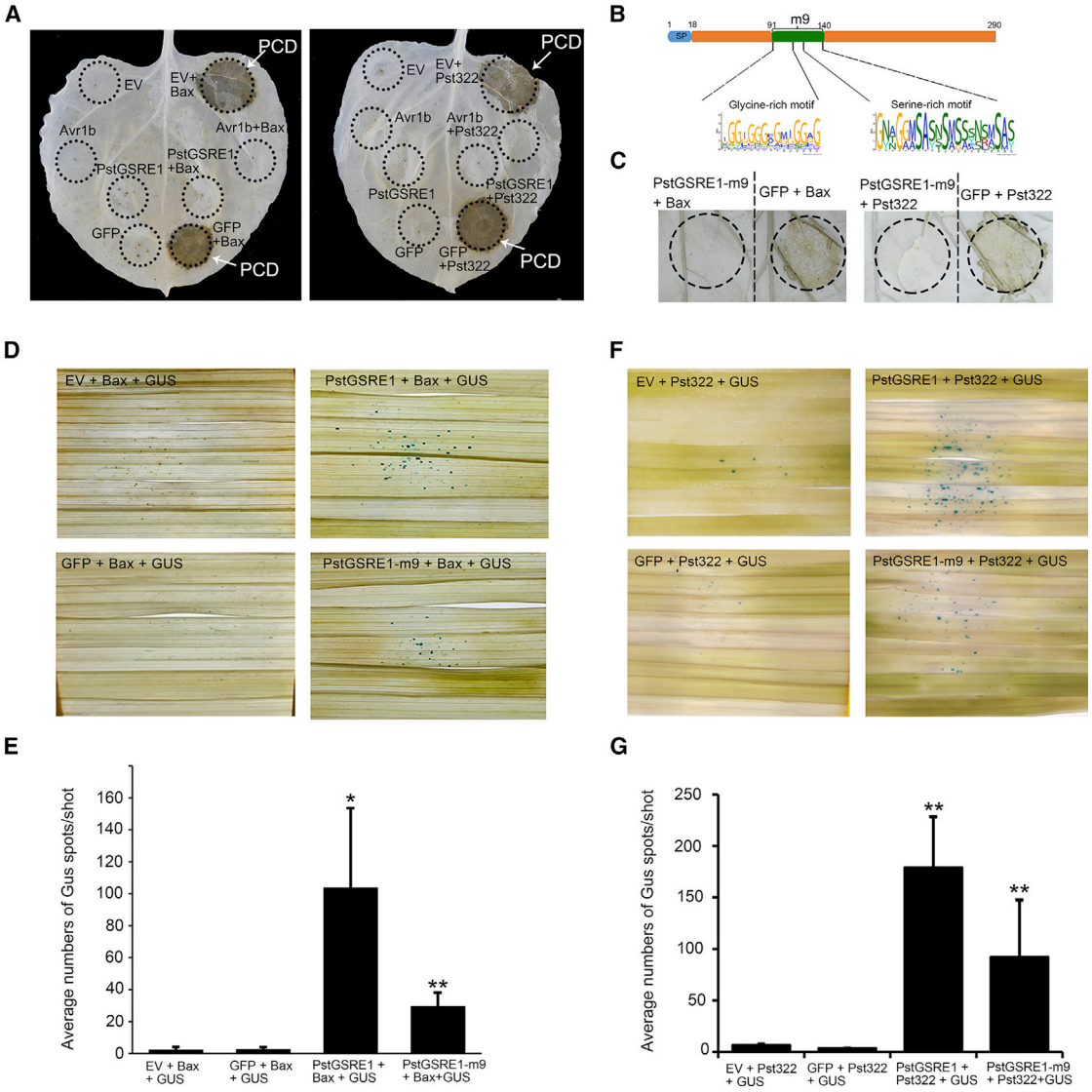

Figure 1. PstGSRE1 Is a Glycine-Serine-Rich Candidate Effector and Its m9 Region Is Responsible for the Suppression of Bax/ Pst322-Induced Cell Death.

(A) Overexpression of *PstGSRE1*-ΔSP in *N. benthamiana* suppresses PCD triggered by Bax (left) or Pst322 (right). *N. benthamiana* leaves were infiltrated with *A. tumefaciens* containing PVX-PstGSRE1, PVX-eGFP, or PVX-Avr1b, either alone or with *A. tumefaciens* cells carrying PVX-Bax or PVX-Pst322, which were infiltrated 24 h later. EV, empty vector.

(B) Structure of the m9 region (91–140 aa) of PstGSRE1 required for suppression of PCD. The motif was predicted by MEME (http://meme-suite.org/). SP, signal peptide.

(C) The m9 region containing the glycine- and serine-rich motif of PstGSRE1 is sufficient for suppression of Bax- and Pst322-induced PCD in *N. benthamiana*.

(D and E) Overexpression of *PstGSRE1* and *PstGSRE1-m9* with *Bax* in wheat leaves using particle bombardment.

(F and G) Overexpression of *PstGSRE1* and *PstGSRE1-m9* with *Pst322* in wheat leaves using particle bombardment.

Leaves in **(D)** to **(G)** were bombarded with the pairs of DNA mixtures indicated. Blue spots indicate living cells, and the average number of GUS spots per shot were counted using ImageJ software. Differences were assessed using Student's *t*-test. $^{*}P < 0.05$, $^{**}P < 0.01$.

strain, YTK12. The fusion of the signal peptide of PstGSRE1 to the mature sequence of SUC2 promoted the successful secretion of invertase, which enables the yeast cells to hydrolyze raffinose and grow on YPRAA medium. The secretion of invertase and the hydrolysis of raffinose into monosaccharides were also confirmed with 2,3,5-triphenyltetrazolium chloride, which reacts with monosaccharides to form the insoluble (red colored) triphenylformazan (Supplemental Figure 2B).

To further examine the function of PstGSRE1, we transiently expressed it in *Nicotiana benthamiana* using agroinfiltration. We observed that PstGSRE1 with or without its signal peptide could suppress PCD triggered by the proapoptotic protein Bax (Figure 1A and Supplemental Figure 3A). Accumulation of PstGSRE1, GFP, and Bax proteins in infiltrated tissue was confirmed by western blot analysis (Supplemental Figure 3B). In addition, PstGSRE1 inhibited PCD induced by an elicitor-like protein, Pst322, from *Pst* (Wang et al., 2012) (Figure 1A and

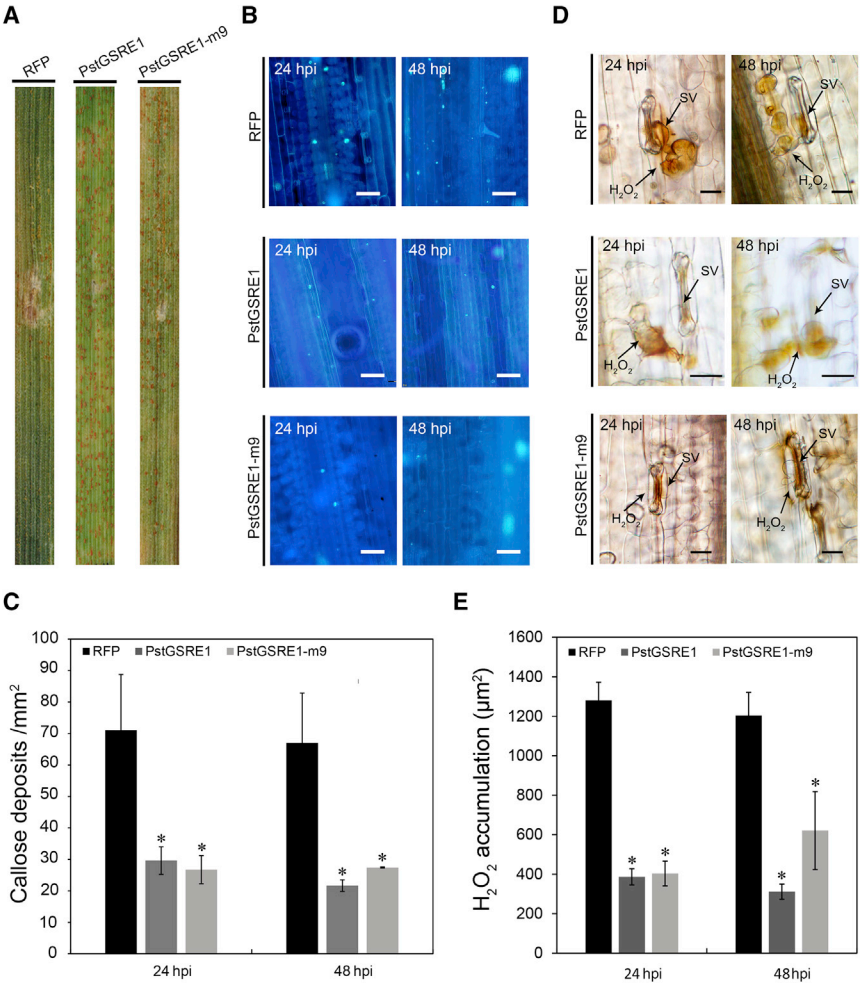

Figure 2. Overexpression of *PstGSRE1* and *PstGSRE1-m9* in Wheat Suppresses PTI-Associated Callose Deposition and H_2O_2 Accumulation.

(A) Phenotypes of wheat leaves inoculated with CYR23 after being injected with *P. fluorescens* strain EtHAn carrying pEDV6-RFP, pEDV6-PstGSRE1, or pEDV6-PstGSRE1-m9 at 14 dpi.

(B) Wheat leaves inoculated as above were examined for callose deposition by epifluorescence microscopy after aniline blue staining. Scale bars, 100 μm.

(C) The average number of callose deposits per mm^2 at 24 hpi and 48 hpi was counted using ImageJ software. Asterisk marks a significant difference at $P < 0.05$.

(D) H_2O_2 production in leaves infiltrated with EtHAn pEDV6-RFP (control), EtHAn pEDV6-PstGSRE1, or EtHAn pEDV6-PstGSRE1-m9 at 24 and 48 hpi with *Pst*. SV, substomatal vesicle. Staining was done using DAB. Scale bars, 20 μm.

(E) The amount of H_2O_2 production was measured by calculating the DAB-stained area at each infection site using DP-BSW software. Values represent the means ± SE of three independent samples. Asterisks indicate a significant difference ($P < 0.05$) relative to the control sample according to Student's *t*-test.

Supplemental Figure 3A). To further analyze the region required for suppression of PCD, we transiently expressed nine deletion mutants of *PstGSRE1* in *N. benthamiana*, after which plants were challenged with Bax. PstGSRE1 mutants m1 to m6 functioned similarly to wild-type PstGSRE1 in suppressing PCD induced by Bax. PstGSRE1-m7 and PstGSRE1-m8, however, lost their PCD-suppression activity (Supplemental Figure 3C). A small region covering aa 91–140 (PstGSRE1-m9) (Figure 1B) was sufficient to suppress PCD (Figure 1C and Supplemental Figure 3C–3E), indicating that the m9 region is essential for the PCD-suppression function of PstGSRE1. Using MEME (Multiple EM for Motif Elicitation), a motif was found in the m9 region that is rich in glycine (34% of m9) and serine (22% of m9) (Figure 1B). Furthermore, PstGSRE1 or PstGSRE1-m9 could also inhibit cell death triggered by Bax (Figure 1D and 1E) or Pst322 (Figure 1F and 1G) as measured using a co-bombardment assay in wheat leaves. Numerous blue spots representing living cells were observed on wheat leaves co-bombarded with pUC-*Bax* or pUC-*Pst322* and the pUC-*Gus* reporter together with pUC-*PstGSRE1* or pUC-*PstGSRE1*-m9. However, only a few blue spots appeared on wheat leaves co-bombarded with pUC-Pst322 and pUC-*Gus* together with the empty vector. Our results indicate that the glycine-serine-rich m9 region of PstGSRE1 is responsible for the suppression of PCD induced by Bax and Pst322.

PstGSRE1 Suppresses Callose Deposition and *Pst*-Induced ROS Accumulation

An important function of fungal effectors is to suppress PTI and/or ETI in order to create a suitable environment for infection. To analyze the ability of PstGSRE1 and PstGSRE1-m9 to suppress PAMP-triggered responses, we used a bacterial type III secretion assay for delivery of fungal effector proteins into wheat (Upadhyaya et al., 2014) to deliver *PstGSRE1* or *PstGSRE1*-m9 into wheat leaves (Figure 2A). Callose deposition triggered by *Pseudomonas fluorescens* strain EtHAn carrying pEDV6-*PstGSRE1* or pEDV6-*PstGSRE1*-m9 was significantly reduced compared with that triggered by the control strain carrying pEDV6-RFP at 24 and 48 h post inoculation (hpi) (Figure 2B and 2C). We further analyzed effector-triggered ROS accumulation upon inoculation of wheat with *Pst* avirulent race CYR23. The results showed that H_2O_2 accumulation was significantly suppressed after transient transformation with EtHAn-*PstGSRE1* or EtHAn-*PstGSRE1*-m9 at 24 and 48 hpi (Figure 2D and 2E). These data indicate that delivery of *PstGSRE1* or *PstGSRE1*-m9 into wheat suppresses PTI-associated callose deposition as well as avirulent *Pst*-induced ROS accumulation in wheat.

Silencing of *PstGSRE1* Significantly Reduces the Virulence of *Pst*

During the interaction between wheat and *Pst* virulent race CYR32, *PstGSRE1* was highly induced at early stages of infection with a maximum transcript level at 24 hpi (Supplemental Figure 4). To investigate the function of PstGSRE1 in *Pst* infection, we used

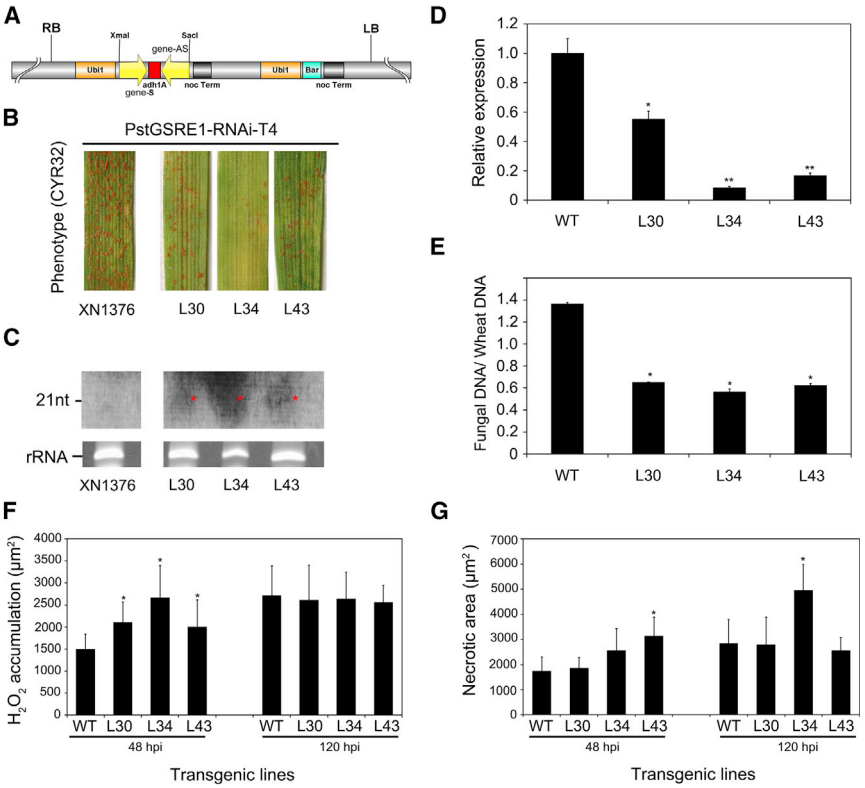

Figure 3. Host-Induced Gene Silencing of *PstGSRE1* Significantly Reduces the Virulence of *Pst* and Increases H_2O_2 Accumulation in Wheat.

(A) Diagram showing the RNAi cassette in the construct pAHC25-*PstGSRE1*-RNAi. Ubi1, maize ubiquitin1 promoter; Adh1, maize alcohol dehydrogenase 1; Noc Term, Nos terminator; Bar, Biolaphos resistance gene; LB, left border; RB, right border.

(B) Phenotypes of second leaves of the fourth generation of wheat plants at 14 dpi with *Pst*.

(C) Expression of small RNAs in T_4 lines L30, L34, and L43 was analyzed by RNA gel blotting. Total RNA was extracted from third leaves pooled from three different plants. RNA blots were hybridized with a gene-specific probe. Bottom: 26S rRNA loading/blotting control. Red asterisk indicates the siRNAs expressed in different transgenic lines.

(D) Relative transcript levels of *PstGSRE1* in different transgenic lines at 48 hpi with *Pst*.

(E) Ratio of fungal to wheat nuclear content determined using the contents of fungal *PstEF1* and wheat *TaEF1* genes, respectively. Genomic DNA was extracted from the second leaf from three different plants at 7 dpi.

(F) Quantification of H_2O_2 accumulation in different transgenic lines at 48 and 120 hpi.

(G) Quantification of necrotic cell death area of different transgenic lines at 48 and 120 hpi.

Values in **(D)** to **(G)** represent the means ± SE of three independent assays. Differences were assessed using Student's *t*-test. $^*P < 0.05$, $^{**}P < 0.01$.

barley stripe mosaic virus (BSMV)-mediated host-induced gene silencing. Two fragments were specifically designed for silencing *PstGSRE1* (Supplemental Figure 5A and Supplemental Table 3). Ten days after virus inoculation, photobleaching was observed in BSMV:*TaPDS*-as treated plants, and all wheat seedlings inoculated with BSMV:γ (control), BSMV:*PstGSRE1*-F, or BSMV:*PstGSRE1*-B displayed mild chlorotic mosaic symptoms, suggesting that the BSMV system functioned properly. After *Pst* inoculation, wheat leaves infected with BSMV:*PstGSRE1*-F or BSMV:*PstGSRE1*-B exhibited a significant reduction in sporulation compared with control plants (Supplemental Figure 5B). In addition, silencing efficiency of leaves infected by BSMV:PstGSRE1-F were reduced to 14%, 11%, and 34% at 24, 48 and 120 hpi, respectively. Leaves infected by BSMV:PstGSRE1-B were reduced to 24%, 16%, and 59% at 24, 48 and 120 hpi, respectively (Supplementary Figure 5C). At 14 days after Pst inoculation of the leaves infected by BSMV:PstGSRE1-F and BSMV:PstGSRE1-B, the area of uredia per leaf area was also reduced by 64.4% and 40.9% compared with the control plants (Supplementary Figure 5D). Moreover, the fungal biomass was significantly reduced by 66% and 76%, respectively, compared with the controls inoculated with BSMV:γ (control) as determined by qPCR (Supplementary Figure 5E). Histological changes in the pathogen were also observed in plants carrying a silencing construct and inoculated with *Pst*, based on staining with wheat germ agglutinin (WGA). As shown in Supplemental Figure 6, hyphal lengths and infection area were significantly reduced relative to those in BSMV:γ-treated leaves at 120 hpi.

To further confirm the virulence function of *PstGSRE1* in *Pst* infection using stable transgenic plants, we prepared the RNA interference (RNAi) construct pAHC25-*PstGSRE1*-RNAi (Figure 3A) and delivered it into wheat cv. XN1376 by particle bombardment. Three T_4 transgenic wheat lines (L30, L34, and L43) containing pAHC25-*PstGSRE1*-RNAi displayed significantly enhanced resistance against *Pst* virulent race CYR32 (Figure 3B). Northern blotting (Figure 3C) was performed to detect *PstGSRE1* small interfering RNAs (siRNAs). The results showed that lines L30, L34, and L43 all contained at least one copy of the transgene (Supplemental Figure 7), and produced siRNAs (~21 nt) (Figure 3C). Transcript levels of *PstGSRE1* during *Pst* infection of transgenic lines L30, L34, and L43 were significantly reduced (Figure 3D). Compared with control plants, fungal biomass in infected leaves of transgenic lines L30, L34, and L43 was significantly reduced (Figure 3E). The formation of mature haustoria and the development of secondary hyphae were investigated by microscopic assessment. At 48 hpi, mycelial morphology and number of hyphal branches showed no difference from the control. However, hyphal lengths during infection of L30 and L34 were significantly reduced at 48 and 120 hpi (Supplemental Figure 8 and Supplemental Table 4). Mycelial morphology appeared normal at 120 hpi, while both the length of infection hyphae and area of infection were significantly reduced in L30 and L34 at 120 hpi (Supplemental Figure 8 and Supplemental Table 4). H_2O_2 accumulation and necrotic cell death area were also measured during *Pst* infection of transgenic plants at 48 and 120 hpi. At 48 hpi, H_2O_2 accumulation was significantly

increased but there was no difference between the transgenic plants and the control at 120 hpi (Figure 3F and Supplemental Figure 9). Hypersensitive cell death was significantly increased, albeit inconsistently (L43 at 48 hpi; L34 at 120 hpi) (Figure 3G and Supplemental Figure 9). These findings indicate that silencing *PstGSRE1* significantly reduced the virulence of *Pst*, suggesting that PstGSRE1 is an important virulence factor.

PstGSRE1 Targets Wheat Transcription Factor TaLOL2

To identify wheat proteins that might be targeted by PstGSRE1 in order to exert its virulence functions, we screened a yeast two-hybrid (Y2H) library constructed from *Pst*-infected wheat leaves, using PstGSRE1 without its signal peptide as bait. As shown in Supplemental Table 5, several candidate targets were identified. As transgenic expression of *PstGSRE1* RNAi constructs significantly increased H_2O_2 accumulation in wheat, we focused on candidate target genes involved in ROS signaling for further study. Two of the candidate target sequences were annotated as ROS-associated Lesion-Simulating Disease 1 (LSD1)-type transcription factors (TraesCS5B01G054000.1 and TraesCS5A02G048900.1). Phylogenetic analysis of TraesCS5B01G054000.1 and TraesCS5A02G048900.1 indicated that they were two of triple homologous gene in wheat and highly similar to OsLOL2 (Xu and He, 2007), and thus we designated TraesCS5B01G054000.1 as TaLOL2 (GenBank: JX135580.1) (Supplemental Figure 10A). Sequence analysis showed that TaLOL2 contains three zinc-finger domains (Supplemental Figure 10B) and that there are three copies in the wheat genome located on chromosomes 5A, 5B, and 5D (Supplemental Figure 10C). To confirm the interaction between TaLOL2 and PstGSRE1, we cloned the open reading frame of *TaLOL2* and the sequence encoding mature *PstGSRE1* into the Y2H vectors pGADT7 and pGBKT7, respectively. An LSD1-type transcription factor, TaLSD1 (Guo et al., 2013), which is homologous to TaLOL2, was used as a negative control. As shown in Figure 4A and 4B, the interaction was confirmed by growth of yeast strain AH109 on selective medium containing 30 mM 3-amino-1,2,4-triazole and staining with X-α-gal. Furthermore, the small fragment of PstGSRE1 capable of suppressing PCD, PstGSRE1-m9, also interacted with TaLOL2 in yeast (Figure 4A and 4B). To further analyze the interaction region, we designed five deletion mutants of TaLOL2 based on the bioinformatics prediction of potential conserved domains (Figure 4A). As shown in Figure 4B, TaLOL2 mutant M5 lacking the C-terminal domain (111–179 aa) failed to interact with PstGSRE1 while mutant M4 retaining only the C terminus interacted with both PstGSRE1 and PstGSRE1-m9. The expression of the above fusion proteins was also detected by western blot (Figure 4C). Thus, we infer that the m9 region of PstGSRE1 interacts with the C-terminal domain of TaLOL2.

To further confirm the interaction of PstGSRE1 with TaLOL2, we expressed recombinant His-PstGSRE1, glutathione *S*-transferase (GST)-TaLOL2, and GST (as a negative control) in *E. coli* strain BL21 and used the *E. coli* crude extracts to perform *in vitro* pull-down assays (Figure 4D). His-PstGSRE1 could be detected in the GST-TaLOL2 but not GST pull-down fractions. Providing further evidence, PstGSRE1 mature protein fused to RFP and TaLOL2 fused to GFP were co-expressed in *N. benthamiana*, and the interaction between them was confirmed using *in planta* co-immunoprecipitation (coIP) with anti-RFP antibodies and western blotting with anti-TaLOL2 antibodies (Figure 4E). Moreover, PstGSRE1-m9 was also proved to interact with TaLOL2 in pull-down and coIP assays (Figure 4F and 4G).

TaLOL2 Positively Regulates Wheat Resistance against *Pst*

To confirm the role of TaLOL2 in the resistance of wheat against *Pst*, we performed qRT–PCR analysis of *TaLOL2* during *Pst* infection. During the interaction between wheat and *Pst*, transcript levels of *TaLOL2* were upregulated and peaked at 120 hpi after inoculation with the avirulent *Pst* race CYR23 (up-regulated by about 6-fold). Moreover, the response dynamics were similar, albeit weaker, during infection with the virulent race CYR31 (Supplemental Figure 10D). In addition, we knocked down expression of *TaLOL2* in wheat using BSMV-mediated virus-induced gene silencing (VIGS). Two specific fragments were designed for silencing *TaLOL2* (Supplemental Figure 11A and Supplemental Table 6). At 10 dpi with virus, plants displayed mild chlorotic mosaic symptoms (Figure 5A). Sporadic uredia appeared on leaves of *TaLOL2*- knock-down plants after inoculation with the avirulent race CYR23, but no uredia were observed on the control plants (Figure 5B). After inoculation with fresh urediospores of virulent *Pst* CYR31, the two *TaLOL2*-silenced lines had more uredia (434 and 572 per leaf area) than the two control plants (258 and 293 per leaf area) (Figure 5C). The relative transcript levels of leaves infected by BSMV:TaLOL2-F were reduced to 49%, 40%, and 63% compare with control plants at 24, 48 and 120 hpi, respectively. Leaves infected by BSMV:TaLOL2-B were reduced to 18%, 30%, and 41% at 24, 48 and 120 hpi, respectively (Supplementary Figure 5C) (Figure 5D). Histological changes in *TaLOL2*-knockdown plants infected with CYR23 were observed by microscopy. As shown in Figure 5E and Supplemental Figure 11B–11D, H_2O_2 accumulation and hypersensitive cell death triggered by *Pst* avirulent race CYR23 were significantly decreased in *TaLOL2*-knockdown plants at 48 and 120 hpi.

To further test the function of *TaLOL2* in wheat defense against *Pst*, we also performed transient delivery of TaLOL2 into wheat using the bacterial T3SS system. At 48 h post infiltration with plasmid-carrying EtHAn strains, wheat plants were inoculated with *Pst* virulent race CYR31. The number of uredia was significantly reduced at 14 dpi (Figure 5F). In addition, the area of H_2O_2 accumulation was significantly increased (Figure 5G). Our results indicate that *TaLOL2* positively regulates wheat resistance against *Pst*.

PstGSRE1 Inhibits TaLOL2-Induced Cell Death by Disrupting Nuclear Translocation of TaLOL2

Previous studies indicated that LSD1-type transcription factors (e.g., *BohLOL1* in *Bambusa oldhamii*) (Yeh et al., 2011) typically function in the nucleus. As shown in Supplemental Figure 12A, cells expressing the TaLOL2-GFP fusion protein show higher fluorescence in nuclei than those expressing GFP alone. TaLOL2 is a member of an LSD transcription factor family, members of which positively (AtLOL1) or negatively (AtLSD1) modulate responses to superoxide-dependent cell death signals in *Arabidopsis* (Epple et al., 2003). To determine

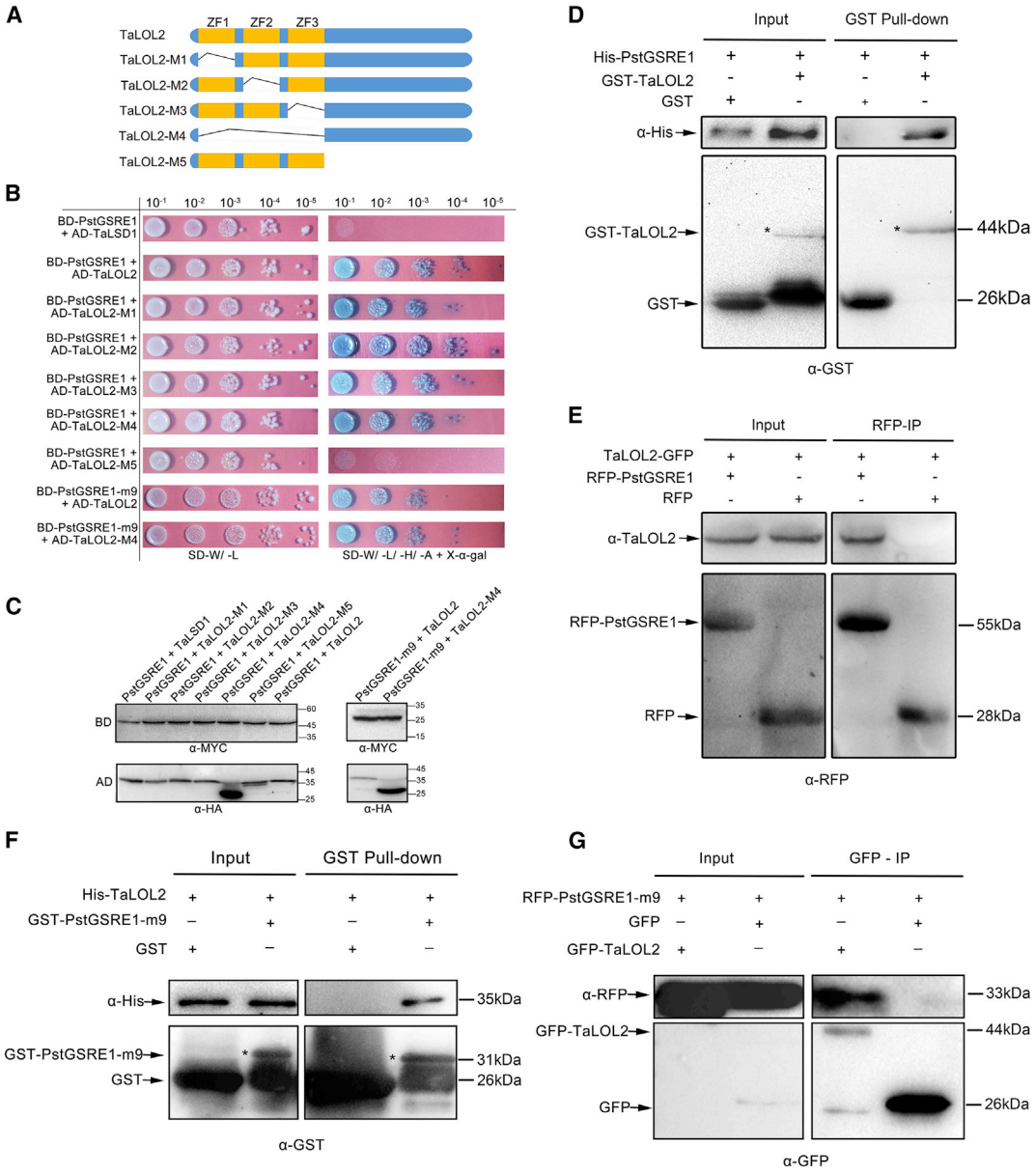

Figure 4. PstGSRE1 Physically Interacts with Wheat TaLOL2 *In Vitro* and *In Vivo*.

(A) Design of pGADT7-TaLOL2 mutants. The blue color indicates TaLOL2 and the yellow color highlights the three zinc-finger domains (ZF1–ZF3).

(B) Y2H analysis of the interaction between PstGSRE1 and TaLOL2. The pGBKT7-PstGSRE1 and pGBKT7-PstGSRE1-m9 proteins both interact with pGBKT7-TaLOL2 and pGBKT7-TaLOL2 mutants (-M1 to -M4) in yeast. Cells of yeast strain AH109 harboring the indicated plasmid combinations were grown on selective medium SD-W/-L or SD-W/-L/-H/-A (SD/-Trp/-Leu or SD/-Trp/-Leu/-His/-Ade containing 20 μg/ml X-α-gal). TaLSD1 was included as a negative control. Plates were photographed 3 days after inoculation.

(C) The western blot assay was used to detect the all the protein in yeast. All the BD-PstGSRE1 and BD-PstGSRE1-m9 were detected by anti-MYC antibodies. All the AD-TaLOL2, its mutants and AD-TaLSD1 were detected by anti-HA tag.

(D) A GST pull-down assay was used to detect the interaction between His-PstGSRE1 and GST-TaLOL2. PstGSRE1 and TaLOL2 were fused to His and GST tags, respectively, and produced in *E. coli*. GST-TaLOL2- or GST-bound resin was incubated with *E. coli* crude extracts containing His-PstGSRE1 and analyzed by western blot. His-PstGSRE1 and GST-TaLOL2 were detected using anti-His tag and anti-GST antibodies, respectively. GST-TaLOL2 is marked by asterisks.

(E) PstGSRE1 interacts with TaLOL2 *in vivo*. Co-immunoprecipitation (IP) was performed on extracts of *N. benthamiana* leaves expressing both RFP-PstGSRE1 and TaLOL2-GFP. RFP was detected by western blot using anti-RFP antibodies. TaLOL2-GFP was detected by western blot using anti-TaLOL2 antibodies.

(F) A GST pull-down assay was used to detect the interaction between GST-PstGSRE1-m9 and His-TaLOL2. GST-PstGSRE1-m9 and His-TaLOL2 were detected using anti-GST tag and anti-His antibodies, respectively. GST-PstGSRE1-m9 is marked by asterisks.

(G) PstGSRE1-m9 interacts with TaLOL2 *in vivo*. Co-immunoprecipitation (IP) was performed on extracts of *N. benthamiana* leaves expressing both RFP-PstGSRE1-m9 and TaLOL2-GFP. RFP was detected by western blot using anti-RFP antibodies. TaLOL2-GFP was detected by western blot using anti-GFP antibodies.

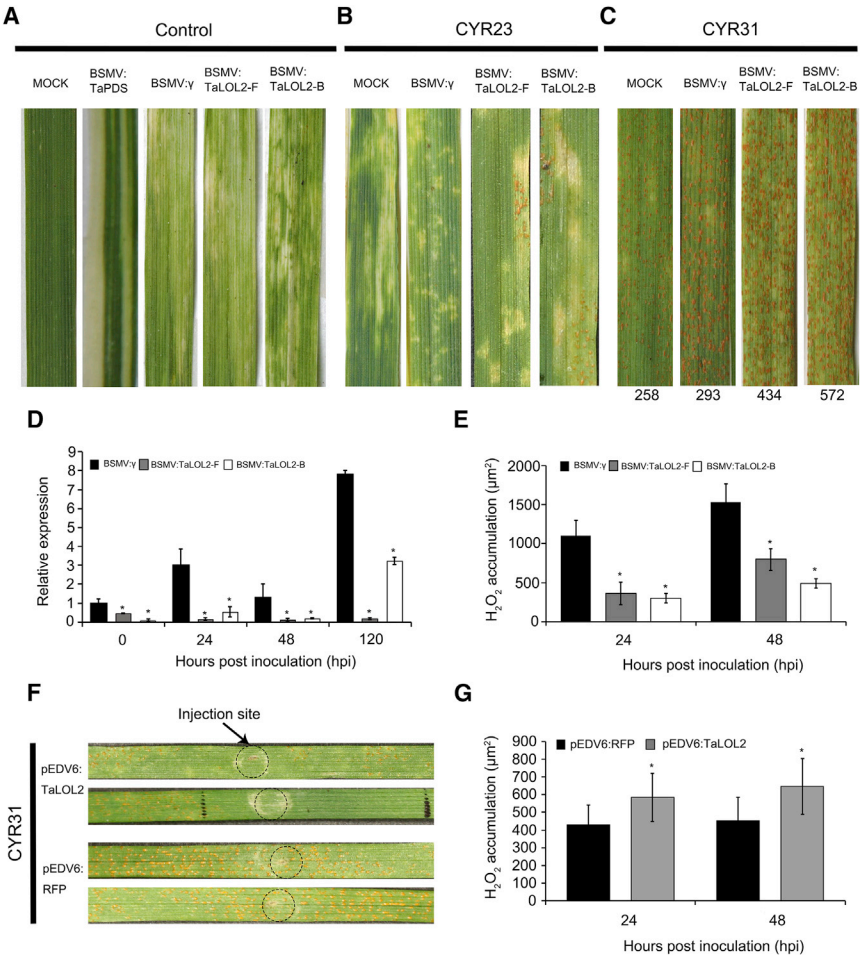

Figure 5. *TaLOL2* Positively Regulates Wheat Resistance against *Pst* in an ROS-Dependent Manner.

(A) Mild chlorotic mosaic symptoms were observed on leaves inoculated with BSMV:γ, BSMV:*TaPDS*-as, or BSMV:*TaLOL2*-F/B at 10 dpi. Mock, wheat leaves treated with 1× Fes buffer.

(B) Phenotypes of fourth leaves challenged with fresh urediospores of *Pst* avirulent race CYR23.

(C) Phenotypes of fourth leaves challenged with fresh urediospores of *Pst* virulent race CYR31. Numbers below leaves indicate the number of uredia. The numbers of uredia were quantified using ImageJ software.

(D) Relative transcript levels of *TaLOL2* in *TaLOL2*-knockdown plants challenged by CYR23 or CYR31. *TaEF1* was used for normalization.

(E) The amount of H_2O_2 accumulation in leaves inoculated with CYR23 was measured by calculating the DAB-stained area at each infection site using DP-BSW software. Values represent means ± SE of three independent assays.

(F) Phenotypes of pEDV6-RFP- and pEDV6-PstGSRE1-treated wheat plants inoculated with the virulent *Pst* race CYR31 at 12 dpi.

(G) Quantification of H_2O_2 accumulation in pEDV6-RFP- and pEDV6-TaLOL2-treated wheat plants inoculated with virulent *Pst* race CYR31 at 24 and 48 hpi.

Values represent means ± SE of three independent samples. Asterisks indicate a significant difference ($P < 0.05$) according to Student's *t*-test.

whether the function of TaLOL2 is associated with PCD, we transiently overexpressed *TaLOL2* in *N. benthamiana* using *Agrobacterium*-mediated transformation. As shown in Supplemental Figure 12B, the expression of TaLOL2 induced obvious PCD in leaves of *N. benthamiana*. When we co-expressed *PstGSRE1* together with *TaLOL2* in *N. benthamiana*, we found that PstGSRE1 could suppress TaLOL2-mediated PCD (Supplemental Figure 12C).

Moreover, we overexpressed *PstGSRE1* or *PstGSRE1*-m9 and *TaLOL2* in *T. aestivum* leaves using single-barreled particle bombardment (Supplemental Figure 12D). When pUC-*PstGSRE1* or pUC-*PstGSRE1*-m9 were co-expressed with pUC-*TaLOL2* and pUC-*GUS* the average number of blue spots, which indicate living cells, was significantly increased compared with control leaves in which empty vectors replaced the pUC-*PstGSRE1* constructs (Supplemental Figure 12E). These results indicate that both PstGSRE1 and PstGSRE1-m9 can suppress TaLOL2-triggered cell death in wheat leaves.

To test whether nuclear localization of TaLOL2 is required for TaLOL2-mediated PCD, we fused a nuclear export signal (NES) to the N terminus of GFP-tagged TaLOL2 (TaLOL2^{NES}). A construct with a mutated NES (TaLOL2^{nes}) was used as a control. The addition of a functional NES caused a strong reduction of TaLOL2-GFP fluorescence in the nucleus of *N. benthamiana* leaves. The agroinfiltration results indicate that the TaLOL2^{NES}-GFP fusion protein could not induce PCD while the mutant TaLOL2^{nes}-GFP fusion protein could induce PCD (Figure 6A and 6B). Proteins of TaLOL2^{NES}-GFP and TaLOL2^{nes}-GFP were detected in total and nuclear protein extracts by western blot analysis (Figure 6C). It thus appears that TaLOL2 must localize to the nucleus to activate cell death. To test whether PstGSRE1 acts to keep TaLOL2 out of the nucleus or whether PstGSRE1 enters the nucleus to block the function of TaLOL2, we transiently co-expressed TaLOL2 with PstGSRE1 fused to a nuclear localization signal (NLS) or to an NES in *N. benthamiana* leaves. The infiltrated sites expressing PstGSRE1^{NLS} showed strong HR, whereas PstGSRE1^{NES}-infiltrated sites showed weaker HR when co-expressed with TaLOL2 (Figure 6D). This clearly shows that cytoplasmic localization of PstGSRE1 is required for the suppression of TaLOL2-induced cell death.

To further verify that PstGSRE1 acts to keep TaLOL2 out of the nucleus, we transiently co-expressed TaLOL2-GFP and RFP-PstGSRE1 or RFP-PstGSRE1-m9 in *N. benthamiana* leaves. Co-expression of TaLOL2-GFP with either RFP-PstGSRE1 or PstGSRE1-m9 caused a distinct change in the localization of TaLOL2 in *N. benthamiana* cells. A wheat transcription factor, TaBZR2, which plays a positive role in the regulation of drought response, was used as nuclear-

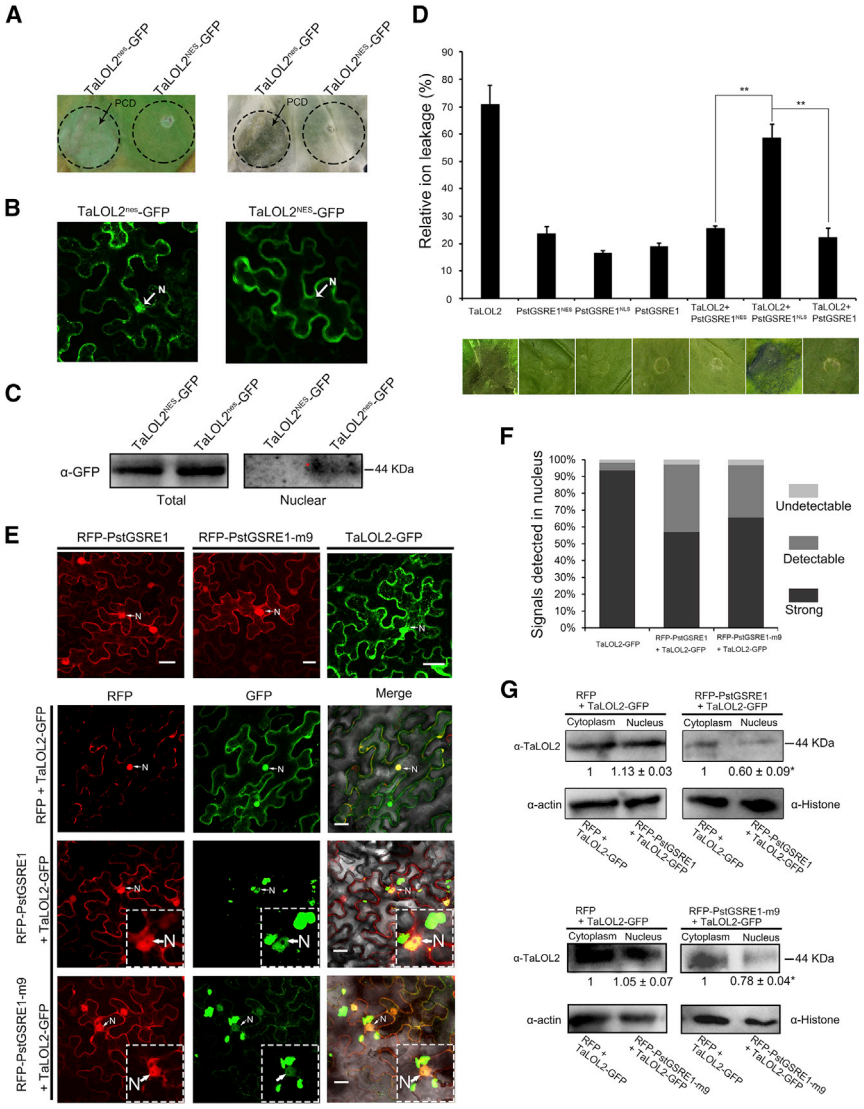

Figure 6. PstGSRE1 Suppresses TaLOL2-Triggered Cell Death by Preventing the Nuclear Localization of TaLOL2.

(A) The nuclear localization of TaLOL2 is required for TaLOL2-induced cell death. Strains with nes- or NES-tagged TaLOL2 PVX constructs were infiltrated into tobacco leaves at a final OD of 0.2. Pictures were taken at 5 dpi.

(B) Confocal microscopy images showing the subcellular localization of TaLOL2 fused with the nuclear export signal NES or the mutant form, nes.

(C) Western blot analysis of TaLOL2^{NES}-GFP and TaLOL2^{nes}-GFP in total and nuclear protein extracts from *N. benthamiana* leaves.

(D) Strains with nuclear localization signal (NLS)-tagged or nuclear export signal (NES)-tagged PstGSRE1 constructs were agroinfiltrated together with TaLOL2 into *N. benthamiana* leaves in a 1:1 ratio and at a final OD of 0.5. Pictures were taken at 6 dpi. The *y* axis shows the average percentage of ion leakage from infiltrated sites, which indicates TaLOL2-induced cell death, at 6 dpi. The average is based on three independent experiments (n ≥ 18). Values represent means ± SE of three independent samples. Double asterisks indicate a significant difference ($P < 0.01$) according to Student's *t*-test.

(E) Co-localization of RFP-PstGSRE1 with TaLOL2-GFP and RFP-PstGSRE1-m9 with TaLOL2-GFP in *N. benthamiana*. In all panels, proteins were expressed in *N. benthamiana* using agroinfiltration. Fluorescence was detected in epidermal cells of the infiltrated leaves by confocal microscopy 48 h after agroinfiltration (prior to any cell death). The RFP-fusion of PstGSRE1 without its signal peptide and the RFP-fusion of PstGSRE1-m9 were uniformly located in the cytoplasm and nucleus; GFP-fusions of TaLOL2 were primarily located in the nucleus, but also in the cytoplasm, often in small punctate structures. When TaLOL2 was expressed together with PstGSRE1 or PstGSRE-m9, the subcellular localization of both PstGSRE1/PstGSRE-m9 and TaLOL2 in non-nuclear bodies. The dotted square shows an enlarged image of the fluorescence around the nucleus. N represents nucleus. Scale bars, 20 μm.

(F) A total of 204, 177, and 183 epidermal cells of *N. benthamiana* expressing TaLOL2-GFP alone, TaLOL2-GFP together with PstGSRE1, and TaLOL2-GFP with PstGSRE1-m9, respectively, were screened for the distribution of fluorescence. The Strong means strong signal in nuclues, the Detectable means partial signal in nuclues and Undetectable means no signal in nuclues.

(G) Western blot analysis of TaLOL2-GFP in cytoplasmic and nuclear extracts from *N. benthamiana* leaves. The cytoplasmic and nuclear fractions were analyzed of TaLOL2-GFP with RFP-PstGSRE1 or RFP-PstGSRE1-m9 by western blot with anti-TaLOL2 antibody, and TaLOL2-GFP with RFP was used as control. Actin and histone H3 were detected as fractionation markers for the cytoplasm and the nucleus, respectively. The relative gray value was calculated using ImageJ for three independent biological replicates.

Asterisks indicate a significant difference compared with TaLOL2-GFP co-expressed with RFP using Student's *t*-test ($P < 0.05$).

targeting protein control (Figure 6E; Supplemental Figure 12F and 12G) (Cui et al., 2019). By itself, TaLOL2-GFP was rather uniformly distributed in the nuclei and to a lesser extent in the cytoplasm. However, in the presence of PstGSRE1 or PstGSRE1-m9, less TaLOL2-GFP was observed in nuclei, and instead a substantial amount of TaLOL2 was localized in large, brightly stained puncta that were often but not always located close to the nuclei. Some of the puncta also included aggregations of PstGSRE1-RFP. PstGSRE1-RFP and PstGSRE1-m9-RFP were also detected in the nucleus. Co-expression with a control effector, Avr1b from *P. sojae*, did not alter the distribution of TaLOL2 (Supplemental Figure 12H and 12I). The percentage of cells expressing only TaLOL2 that exhibited clear and strong fluorescence in the nucleus was about 90%, whereas when TaLOL2 was co-expressed together with PstGSRE1 this percentage was decreased to 57% (Figure 6F). Western blot analysis of cytoplasmic protein and nuclear protein extracts from *N. benthamiana* leaves co-expressing RFP-PstGSRE1 or RFP-PstGSRE1-m9 and TaLOL2-GFP was also performed. Compared with the co-expressing of TaLOL2-GFP and RFP in *N. benthamiana* (control), the TaLOL2 protein level in the

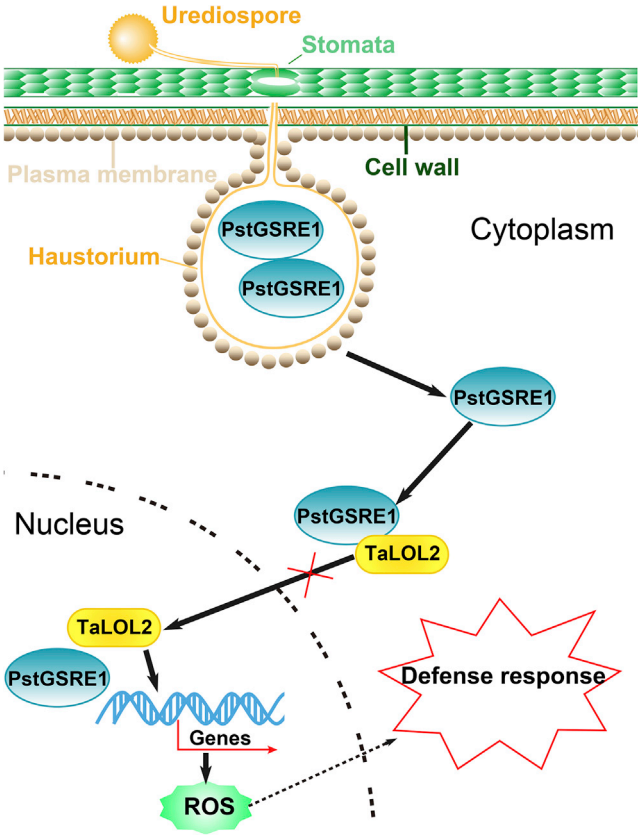

Figure 7. A Working Model Illustrating How PstGSRE1 Suppresses ROS-Associated Wheat Immunity by Interfering with Nuclear Localization of TaLOL2.

During infection, *Pst* produces haustoria, through which effectors are secreted and translocated into host cells. In the initial biotrophic phase, PstGSRE1 acts as an important virulence factor to enhance *Pst* colonization and infection. When PstGSRE1 is secreted by *Pst* and is translocated from the haustorium into the host cell, it targets TaLOL2 and blocks the nuclear localization of TaLOL2, preventing TaLOL2 from carrying out its normal role of activating ROS-mediated HR and disease resistance during the interaction between wheat and *Pst*.

nuclear fraction was reduced in presence of RFP-PstGSRE1 and RFP-PstGSRE1-m9 (relative gray level reduced to 0.60- and 0.78-fold, respectively) (Figure 6G). Taken together, PstGSRE1 acts to keep TaLOL2 out of the nucleus to block the function of TaLOL2.

DISCUSSION

In this study, we have identified a glycine-serine-rich effector, PstSGRE1, from stripe rust that binds to the wheat transcription factor TaLOL2. Expression of *PstGSRE1* siRNA in stable wheat transformants could confer resistance against *Pst* (Figure 3), confirming the importance of this effector for stripe rust infection and identifying a strategy for improving wheat stripe rust resistance. *PstGSRE1* is strongly expressed during early infection (Supplemental Figure 4). PstGSRE1 and its glycine-serine-rich m9 region can suppress PTI-associated ROS and callose deposition in wheat (Figure 2) and also suppress Pst322- and Bax-triggered cell death in wheat and *N. benthamiana* (Figure 1). TaLOL2 is an LSD1-like transcription factor (Supplemental Figure 10). Our study confirmed that, like *Arabidopsis* AtLOL1 (Epple et al., 2003), TaLOL2 plays a positive role in host resistance involving ROS signaling. Overexpression of *TaLOL2* in wheat triggers elevated ROS production (Figure 5G) and cell death (Supplemental Figure 12D) and decreases *Pst* infection (Figure 5F). In contrast, silencing of *TaLOL2* in wheat increases susceptibility to both virulent and avirulent races of *Pst* (Figure 5A–5C), and reduces ROS production (Figure 5E and Supplemental Figure 11B) and localized necrosis (Figure 5; Supplemental Figure 11C and 11D) during infection with an avirulent *Pst* race. PstGSRE1 appears to modify the subcellular localization of TaLOL2 to prevent it from promoting immunity (Figures 6 and 7).

In rust fungi, PstGSRE1 and its homologs form a large family that is conserved among different *Pst* races, and to a considerable extent also among stripe, leaf, and stem rust pathogens. GSREs are defined as small proteins (less than 300 aa) with high glycine and/or serine contents (glycine residues representing more than 11% of aa and serine residues more than 19%). GSREs from various pathogens were found to play important and even decisive roles in infection (Golovkin and Reddy, 1998; Chi et al., 2009; Mangeon et al., 2010; Zhang and Xu, 2014; Nishimura et al., 2016; Martínez-Cruz et al., 2018), but few of them have been characterized in *Pst*. The m9 region of PstGSRE1, containing the glycine-serine-rich motif (91–140 aa), was found to be responsible for the suppression of Bax-induced PCD in tobacco leaves and Pst322-induced cell death in wheat leaves as well as for binding to TaLOL2.

ROS have been proposed to orchestrate the establishment of plant defenses following HR (Lamb and Dixon, 1997; Coll et al., 2011). HR is very effective against obligate biotrophic pathogens. Secreting effectors to suppress or delay HR of the host is an important strategy for successful infection and colonization by obligate biotrophic pathogens. Both PTI and ETI responses can include PCD. Recognition of PAMPs initiates PTI, while recognition of specific pathogen effector molecules can initiate ETI. In animal cells, increased ROS levels are a hallmark of a form of PCD called necroptosis, while in plant cells, ROS have been identified as playing a key role in the development of HR and systemic immunity (Coll et al., 2011). PstGSRE1 was able to suppress ROS accumulation induced by the avirulent *Pst* race CYR23 and could depress the EtHAn-induced deposition of callose. Like PstGSRE1, the rust effectors PEC6 and PSTha5a23 were also reported to be involved in the suppression of callose deposition and ROS accumulation (Cheng et al., 2016; Liu et al., 2016).

PstGSRE1 physically interacts with TaLOL2, a zinc-finger-type LSD1-like transcription factor in wheat. LSD genes were discovered from studies of the lesion-simulating disease resistance class of *Arabidopsis* mutants (Mühlenbock et al., 2008), and are all involved in ROS-induced cell death. In *Arabidopsis*, *LSD1* encodes a negative regulator of PCD while the *LSD1* paralog *LOL1* acts as a positive regulator of cell death (Epple et al., 2003). *LSD1* and *LOL1* have antagonistic effects on copper-zinc superoxide dismutase accumulation. TaLOL2 contains three internally conserved plant-specific zinc-finger domains but does not have a conventional NLS sequence. However, we observed partial nuclear localization of TaLOL2 in wheat

protoplasts and *N. benthamiana* cells and found that nuclear localization of TaLOL2 is required for TaLOL2-induced cell death in *N. benthamiana*. By silencing *TaLOL2* in wheat leaves using BSMV-VIGS and bacterial delivery of TaLOL2 into wheat tissue, TaLOL2 was determined to be a positive regulator of wheat resistance to *Pst* in an ROS-associated manner. Targeting an important immune regulator such as TaLOL2 by an effector such as PstGSRE1 would be an effective strategy for *Pst*. *TaLOL2* is a homolog of a rice *LSD1-like* gene (*OsLOL2*). Silencing of *OsLOL2* made rice more susceptible to bacterial blight, and overexpression of *OsLOL2* enhanced rice resistance against bacterial blight (Xu and He, 2007). Overexpression of *OsLOL2* in transgenic tobacco made the plants more resistant to *Pseudomonas syringae* pv. *tabaci* (Bhatti et al., 2008) and to *Ralstonia solanacearum* (Bhatti et al., 2011). Thus OsLOL2, like TaLOL2 appears to be a positive regulator of defense. In *Arabidopsis*, the protein most similar to TaLOL2 and OsLOL2 is LSD1 itself (TaLOL2 has 57% identify to LSD1 and 42% to LOL1). Thus, although LSD1 is a negative regulator of ROS-associated cell death in *Arabidopsis*, its closest homologs in rice and wheat appear to be positive regulators.

Defense-related gene expression regulates a wide variety of physiological processes, including cuticular wax biosynthesis (Bi et al., 2017), stomatal closure (Tan et al., 2017), ROS detoxification (Torres, 2010), and structural alterations in plasma membranes. Thus, transcription factors that regulate plant defense are a logical target for effectors. Members of the bacterial family of AvrBs3 effectors act as transcription factors to modulate host signaling pathways (Kay et al., 2007). Another bacterial effector, AvrRps4, interacts with WRKY transcription factors (Sarris et al., 2015). PpEC23 from *Phakopsora pachyrhizi* targets transcription factor GmSPL12l to suppress host defense response (Qi et al., 2016). RxLR effector Pi03192 from *Phytophthora infestans* disturbs translocation of NAC transcription factors from the endoplasmic reticulum to the nucleus (Hazel et al., 2013). As shown in Figure 7, *PstGSRE1* expression induces partial relocalization of TaLOL2 and reduces the amount of TaLOL2 in nuclei. In addition, expression of *PstGSRE1* in plant cells results in repression of defense and cell death-associated responses. TaLOL2 lacks a detectable NLS, so it remains to be determined how TaLOL2 traffics to the nucleus.

RNAi is an effective tool to characterize gene functions in biotrophic fungi (Nowara et al., 2012). The expression of host double-stranded RNAs targeted toward fungal transcripts in several crop plants has been reported to increase resistance against phytopathogenic fungi, including *Pst* (Qi et al., 2017; Zhu et al., 2017). BSMV-mediated transient silencing of *PstGSRE1* significantly reduced virulence of *Pst*. Transgenic lines carrying *PstGSRE1* RNAi constructs exhibited genetically stable resistance to *Pst* in the T_4 generation. Moreover, cytological and molecular observations showed that the expression of siRNAs targeting *PstGSRE1* in wheat resulted in an enhanced oxidative burst and increased necrosis at infection sites. Thus, PstGSRE1 contributes significantly to plant infection and the virulence of *Pst*.

In summary, we have identified an important virulence effector, PstGSRE1, in *Pst* that blocks nuclear accumulation of the wheat transcription factor TaLOL2 to modulate ROS-associated defense responses. To our knowledge, this is the first direct evidence demonstrating that an effector in *Pst* targets transcriptional regulators to suppress plant immunity. Stable wheat transformants expressing *PstGSRE1*-silencing RNAs showed increased resistance to stripe rust, pointing to novel strategies for protecting the wheat crop.

METHODS

Biological Materials, Growth Conditions, and Fungal Inoculation

Wheat cultivar (cv.) Suwon11 (Su11) is resistant to CYR23 but highly susceptible to CYR31; this system was used for qRT–PCR and BSMV-VIGS (Wang et al., 2012). Wheat cv. XiNong 1376 (XN1376) was used for transformation. *Pst* races CYR32 (virulent on Su11 and XN1376), CYR31 (virulent on Su11), and CYR23 (avirulent on Su11) (Kang et al., 2002) were used in this study. Plant cultivation and inoculation with *Pst* were performed as previously described (Qi et al., 2017). Fresh urediospores of *Pst* race CYR23 were obtained from the leaves of wheat cv. Thatcher (MX169) and those of CYR31 and CYR32 were obtained from wheat cv. Su11.

Plasmid Construction and Plant Transformation

cDNA of *PstGSRE1* was cloned from *Pst* race CYR32 and *TaLOL2* was cloned from Su11. Coding sequences of *PstGSRE1*, *PstGSRE1*-m9, *TaLOL2*, and mutant variants were ligated into pSUC2T7M13ORI (for yeast signal sequence trap), pGR107-PVX (for transient expression in tobacco), pEDV6 (for T3SS-mediated overexpression) (Cheng et al., 2016), pCAM1301-RFP (for co-expression assays) (Goodin et al., 2010), pCold TF (containing a His tag for protein expression), or pEGX4T-1 (containing a GST tag for protein expression) using the appropriate restriction enzymes.

For VIGS assays, specific cDNA fragments of *PstGSRE1* and *TaLOL2* were predicted by si-Fi software and then inserted into the BSMV-γ vector (Cheng et al., 2016). For Y2H assays, the coding sequences or deletion mutants of *PstGSRE1* and *TaLOL2* were prepared using the appropriate restriction enzymes (Supplemental Table 7) and ligated into the pGADT7 and pGBKT7 vectors. Fragments used to generate PstGSRE1-RNAi were synthesized by Nanjing Genewiz (Nanjing, China) and ligated into pAHC25. All recombinant plasmids were verified by sequencing. For coIP, the coding sequences of *TaLOL2* and *PstGSRE1* or *PstGSRE1*-m9 were ligated into pSOL2094 (containing GFP) and pCAM1301-RFP (Du et al., 2015). For fusing NES (NEL ALK LAG LDI NKA ACG AGC TTG CAT TAA AGC TCG CTG GTC TTG ATA TTA ACA AG) or mutated NES (nes) (NEL ALK aAG aDa NKA ACG AGC TTG CAT TAA AGG CAG CTG GTG CAG ATG CTA ACA AG) peptides to TaLOL2 and PstGSRE1, the forward or reverse primers were extended with sequences encoding the NES/nes peptides at the N terminus. For fusing NLS (PKK KRK VED P C CTA AAA AGA AGC GTA AGG TTG AGG ACC CT) or mutated NLS (nls) (PKN KRK VED PCC TAA AAA CAA GCG TAA GGT TGA GGA CCC T) peptides to TaLOL2 and PstGSRE1, the sequences of NLS/nls added to primers at the N terminus. Ion-leakage measurement assay was performed as previously described (Du et al., 2015).

Sequence Analysis of *PstGSRE1* and *TaLOL2*

The signal peptide of PstGSRE1 was predicted using SignalP4.0 (http://www.cbs.dtu.dk/services/SignalP/). Glycine/serine-rich motifs of PstGSRE1 were analyzed by MEME (http://meme-suite.org/). The NCBI conserved domain database (https://www.ncbi.nlm.nih.gov/cdd/) was used to identify domains. *TaLOL2* alleles from chromosomes 5AL, 5BL, and 5DL were obtained from the wheat UGRI genome database (https://urgi.versailles.inra.fr/).

Yeast Two-Hybrid Screens

Recombinant pGBKT7-*PstGSRE1* and pGADT7-cDNA libraries (Clontech, Mountain View, CA, USA) were co-transformed into yeast strain AH109 using the lithium acetate method according to the Yeast Protocols Handbook (Clontech). For interaction analysis of PstGSRE1 and TaLOL2 in yeast, recombinant pGBKT7 containing *PstGSRE1* or *PstGSRE1*-m9 and pGADT7 containing *TaLOL2*, or its mutants (TaLOL-M1, TaLOL-M2, TaLOL-M3, TaLOL-M4, TaLOL-M5) were co-transformed into yeast strain AH109. The presence of both plasmids was confirmed by growth on SD-Leu-Trp, and interactions were tested by plating on SD-Leu-Trp-His-Ade containing X-α-gal. Yeast transformation and interaction tests were performed following the instructions in the Yeast Protocols Handbook (Clontech).

Agrobacterium tumefaciens Infiltration Assays, Confocal Microscopy, and Particle Bombardment

Agrobacterium tumefaciens strain GV3101 carrying binary vectors was cultured on lysogeny broth plates supplemented with appropriate antibiotics at 28°C. For co-expression assays, 4-week-old *N. benthamiana* plants were infiltrated with *A. tumefaciens* containing pCAM1301-RFP-PstGSRE1, GFP-TaLOL2, and the P19 silencing suppressor in a 2:2:1 ratio with a final OD_{600} = 0.6. After 2 days (before cell death could develop), infiltrated areas of the leaves were excised and examined with an Olympus FV3000 confocal laser microscope (Olympus, Tokyo, Japan). Fluorescence of GFP was elicited at 514 nm and detected at 520–540 nm. Fluorescence of RFP was excited at 561 nm and detected at 590–630 nm. To assay the suppression of Bax-/Pst322-induced plant cell death, we infiltrated *A. tumefaciens* cells carrying PVX-PstGSRE1 or its derivatives into *N. benthamiana* leaves followed 24 h later by inoculation at the same site with *A. tumefaciens* cells containing PVX-Bax/PVX-Pst322. Symptoms were recorded at 5 dpi. For protein extraction, *N. benthamiana* leaves were frozen in liquid nitrogen 2 days after agroinfiltration and ground to a fine powder with a mortar and pestle. Protein extraction and nuclear-cytoplasmic fractionation were performed as described by Wang et al. (2011).

For wheat leaf co-bombardment, leaves from 7-day-old plants of Su11 were cut into segments (5 cm) and fixed in dishes with agar medium, then these dishes were shot with the Bio-Rad He/1000 single-barreled particle delivery system. Shooting, staining, and bleaching methods were performed according to a previous study (Wang et al., 2012). A large number of GUS (β-glucuronidase) spots could be observed by microscopy, and the significance of differences between different treatments was analyzed. Each assay consisted of seven shots and was conducted at least twice.

GST Pull-Down Assay

Recombinant plasmids *PstGSRE1*-pCold or *PstGSRE1*-m9-pGEX4T-1 and *TaLOL2*-pGEX4T-1 or *TaLOL2*-pGEX32a were separately transformed into *E. coli* strain BL21. The *E. coli* crude extracts containing the TaLOL2-GST or *PstGSRE1*-m9-GST fusion proteins were incubated with 50 μl of glutathione–agarose beads (GE Healthcare Life Science, Marlborough, MA, USA) at 4°C for 2 h. The supernatant was removed, and the beads were washed three times with ice-cold phosphate-buffered saline (PBS). Beads were then incubated with the *E. coli* crude extract containing the His-PstGSRE1 or His-TaLOL2 proteins at 4°C for 2 h. After washing six times with PBST (PBS containing 0.05% Tween 20), beads were suspended in SDS sample loading buffer and heated to 100°C for 5 min for western blot analysis using anti-His antibody (Sungene Biotech, Tianjing, China).

Co-immunoprecipitation Assays

Leaves of 4- to 6-week-old *N. benthamiana* plants were agroinfiltrated with pCAM1301-RFP-PstGSRE1, pCAM1301-RFP-PstGSRE1-m9, psol2095-TaLOL2 (and pCAM1301-RFP as the control), and the agrobacterium with P19 silencing suppressor was added in a 1:1 ratio at a final OD_{600} = 0.6 for each construct. Two days after agroinfiltration, the leaves were frozen in liquid nitrogen and ground to a fine powder using a mortar and pestle. Proteins were extracted using RIPA lysis buffer and a protease inhibitor cocktail (Sigma-Aldrich) by mixing 1 g of leaf tissue with 2 ml of lysis buffer. The samples were centrifuged at 4°C for 15 min at 14 000 *g* and the supernatant was transferred to a new tube. Two milliliter Two milligrams of total protein extract was incubated at 4°C for 2 h with 20 μl of RFP-Trap A/GFP-Trap beads (Chromotek, Planegg-Martinsried, Germany). The beads were then collected by centrifugation at 2500 *g* and washed five times in 1 ml of washing buffer (10 mM Tris–Cl [pH 7.5], 150 mM NaCl, and 0.5 mM EDTA). Finally, the beads in a 60-μl volume of wash buffer were mixed with 20 μl of 4× loading buffer, heated at 100°C for 5 min, and centrifuged for 5 min at maximum speed. The solubilized proteins were then loaded on a gel or stored at −20°C.

Western Blotting

Proteins were separated by SDS–PAGE. Gels were blotted onto a PVDF membrane (Merck Millipore, Burlington, MA, USA) using transfer buffer at 64 V for 2 h. Membranes were blocked for 1 h at room temperature, followed by washing. The antibodies anti-PstGSRE1 (1:2000; #ZC045GB06P1, PTM BioLabs), anti-TaLOL2 (1:2000; #ZC093H822P2, PTM BioLabs), anti-GFP (1:2000; #A02020, Abbkine), anti-RFP (1:2000; #A02120, Abbkine), anti-Bax (1:2000; #ab182733, Abcam), anti-His (1:3000; #A02050, Abbkine), or anti-GST (1:2000; #A02030, Abbkine) were added, and the membranes were incubated at 4°C overnight, followed by three washes. Membranes were then incubated with goat anti-mouse antibody (#ab6789, Abcam), or goat anti-rabbit (ab205718#, Abcam) at a ratio of 1:10 000 in blotting buffer at room temperature for 2 h. After washing three times, membranes were incubated with chemiluminescence horseradish peroxidase substrate (#WBKLS0100, Merck Millipore) for 5 min and visualized by excitation at 780 or 800 nm.

BSMV-Mediated Virus- or Host-Induced Gene Silencing

Capped *in vitro* transcripts were prepared from linearized plasmids, BSMV:γ:*TaPDS*-as, BSMV:γ:*PstGSRE1*-F, BSMV:γ:*PstGSRE1*-B, BSMV:γ:*TaLOL2*-F, BSMV:γ:*TaLOL2*-B, BSMV:γ, BSMV:α, and BSMV:β, using the Message Machine T7 *in vitro* transcription kit (Ambion, Austin, TX, USA) according to the manufacturer's instructions. The silencing of the wheat phytoene desaturase gene (*TaPDS*) was used as positive control. BSMV:γ and 1× Fes buffer were used as negative controls. Plant cultivation and inoculation with BSMV were performed as previously described (Qi et al., 2017). The types of stripe rust infection were examined at 15 dpi. For RNA isolation and histological observation, leaves inoculated with *Pst* were sampled at 0, 24, 48, and 120 hpi.

Bacterial T3SS-Mediated Overexpression in Wheat Plants

The pEDV6-*PstGSRE1*, pEDV6-*PstGSRE1*-m9, and pEDV6-*TaLOL2* constructs were transformed into *P. fluorescens* strain EtHAn by electroporation. pEDV6-GFP was used as a control. Infiltration into wheat leaves was performed according to a previous study (Jiang and Tyler, 2012). For determination of the involvement in *Pst* pathogenicity or host defense response, the second leaves of wheat plants inoculated with pEDV6-*PstGSRE1*, pEDV6-*PstGSRE1*-m9, or pEDV6-*TaLOL2* were challenged with *Pst* avirulent race CYR23. Inoculated leaves were sampled at 24 and 48 hpi for H_2O_2 measurements determined by 3,3′-diaminobenzidine (DAB) staining. For examination of the suppression of callose deposition, wheat plants inoculated with pEDV6-*PstGSRE1*, pEDV6-*PstGSRE1*-m9, or pEDV6-RFP were sampled at 48 hpi. Leaves were detached and cleared in acetic acid/ethanol (1:1) for 24 h with several changes. Cleared leaves were rinsed in 50% ethanol twice for 15 min each, water for 10 min, 0.5 M NaOH for 10 min, water for 10 min, and finally with 67 mM K_2HPO_4 (pH 9.0) for 1 h. Leaf samples were stained with 0.05% aniline blue in 67 mM K_2HPO_4 (pH 9.0) overnight in darkness. Leaves were rinsed in water, mounted in 50% glycerol, and examined under an Olympus BX-53 fluorescence microscope (Olympus) using a DAPI

filter. Images were acquired using a constant setting with a 1000-ms exposure time. The number of callose deposits was quantified using ImageJ software (Duan et al., 2018).

Cytological Observations of Fungal Growth and Host Response

Leaf segments were fixed and decolorized in a mixture of acetic acid/ethanol (1:1) for 3 days. Autofluorescence of mesophyll cells was observed to determine necrotic death area using epifluorescence microscopy (excitation filter, 485 nm; dichromic mirror, 510 nm; barrier filter, 520 nm). H_2O_2 accumulation was detected by staining with DAB (Amresco, Solon, OH, USA). Hyphae were stained with WGA conjugated to Alexa-488 (Invitrogen, Carlsbad, CA, USA) and observed under blue-light excitation (excitation wavelength 450–480 nm, emission wavelength 515 nm). Only the site where an appressorium had formed over a stoma was considered to be a successful penetration. A minimum of 50 infection sites were examined on each of five randomly selected leaf segments for every treatment.

Northern Blotting

Northern blotting experiments were performed as previously described (Zhu et al., 2017). Approximately 20 μg of total RNA was subjected to electrophoresis on a denaturing 19% polyacrylamide gel, transferred to Nytran Super Charge Nylon Membranes (Schleicher and Schuell MicroScience), and crosslinked using a Stratagene UV Cross Linker. The membranes were prehybridized with PerfectHyb (Sigma-Aldrich) and hybridized with the P32-labeled DNA probes overnight in PerfectHyb buffer (Sigma-Aldrich). The membranes were autoradiographed on X-OMAT BT film (Carestream Health) after rinsing with washing buffer. rRNA was used as a loading control.

Statistical Analyses

Statistical analyses of each treatment were performed with the statistical software package IBM SPSS Statistics version 21 (IBM SPSS Statistics, Armonk, NY, USA).

ACCESSION NUMBERS

Sequence data from this article can be found in the wheat UGRI genome database (https://urgi.versailles.inra.fr/) and Genome Bank Data Library (https://www.ncbi.nlm.nih.gov/) under accession numbers MH426738, TraesCS5B01G054000.1, TraesCS5A02G048900.1, and JX135580.1.

SUPPLEMENTAL INFORMATION

Supplemental Information is available at *Molecular Plant Online*.

FUNDING

This study was financially supported by the National Natural Science Foundation of China (31972224, 31430069, and 31620103913), the National Key R&D Program of China (2018YFD0200402), and the 111 Project from the Ministry of Education of China (no. B07049).

AUTHOR CONTRIBUTIONS

Jun Guo, B.M.T., and Z.-S.K. designed the research; T.Q., Jia Guo, P.L., F.-X.H., C.-P.W., and M.-A.I. performed the research; Jia Guo and T.Q. contributed bioinformatics analysis; T.Q., Jia Guo, P.L., and F.-X.H. analyzed the data; T.Q., Jun Guo, Z.-S.K., B.M.T., and Jia Guo wrote the paper. All authors commented on the article before submission.

ACKNOWLEDGMENTS

We thank Professor Larry Dunkle and Professor Ralf T. Voegele for editing the manuscript, and Professor Daolong Dou for helpful suggestions. We thank Drs. Yu Du and Biao Gu for kindly providing yeast stain YTK12 and vectors pSUC2T7M13ORI and pSOL2094-GFP, and Jiankang Zhu for help with northern blots. No conflict of interest declared.

Received: April 23, 2019
Revised: September 29, 2019
Accepted: September 29, 2019
Published: October 9, 2019

REFERENCES

Bhatti, K.H., Xu, C., Wu, J., and He, C. (2008). Overexpression of rice *OsLOL2* gene confers disease resistance in tobacco to *Pseudomonas syringae* pv. *tabaci*. Prog. Nat. Sci. **18**:807–812.

Bhatti, K.H., Shah, A., Iqbal, M., Iqbal, T., and Jiahe, W. (2011). Transgenic tobacco with rice zinc-finger gene *OsLOL2* exhibits an enhanced resistance against bacterial-wilt. Australas. Plant Pathol. **40**:133–140.

Bi, H.H., Luang, S., Li, Y., Bazanova, N., Borisjuk, N., Hrmova, M., and Lopato, S. (2017). Wheat drought-responsive WXPL transcription factors regulate cuticle biosynthesis genes. Plant Mol. Biol. **94**:15–32.

Büttner, D., and Bonas, U. (2003). Common infection strategies of plant and animal pathogenic bacteria. Curr. Opin. Plant Biol. **6**:312–319.

Chen, H., Chen, J., Li, M., Chang, M., Xu, K., Shang, Z., Zhao, Y., Palmer, I., Zhang, Y., McGill, J., et al. (2017a). A bacterial Type III effector targets the master regulator of salicylic acid signaling, NPR1, to subvert plant immunity. Cell Host Microbe **22**:777–788.

Chen, J., Upadhyaya, N.M., Ortiz, D., Sperschneider, J., Li, F., Bouton, C., Breen, S., Dong, C., Xu, B., Zhang, X., et al. (2017b). Loss of *AvrSr50* by somatic exchange in stem rust leads to virulence for *Sr50* resistance in wheat. Science **358**:1607–1610.

Cheng, Y., Wu, K., Yao, J., Li, S., Wang, X., Huang, L., and Kang, Z.S. (2016). PSTha5a23, a candidate effector from the obligate biotrophic pathogen *Puccinia striiformis* f. sp. *tritici*, is involved in plant defense suppression and rust pathogenicity. Environ. Microbiol. **19**:1717–1729.

Chi, M., Park, S., Kim, S., and Lee, Y. (2009). A novel pathogenicity gene is required in the rice blast fungus to suppress the basal defenses of the host. PLoS Pathog. **5**:e1000401.

Coll, N.S., Epple, P., and Dangl, J.L. (2011). Programmed cell death in the plant immune system. Cell Death Differ. **18**:1247–1256.

Cui, X., Gao, Y., Guo, J., Yu, T., Zheng, W., Liu, Y., Chen, J., Xu, Z., and Ma, Y. (2019). BES/BZR transcription factor TaBZR2 positively regulates drought responses by activation of TaGST1. Plant Physiol. **180**:605–620.

Dangl, J.L., and Jones, J.D. (2001). Plant pathogens and integrated defense responses to infection. Nature **411**:826–833.

Dong, S., Yin, W., Kong, G., Yang, X., Qutob, D., Chen, Q., Kale, S.D., Sui, Y., Zhang, Z., and Dou, D. (2011). *Phytophthora sojae* avirulence effector Avr3b is a secreted NADH and ADP-ribose pyrophosphorylase that modulates plant immunity. PLoS Pathog. **7**:e1002353.

Dou, D., and Zhou, J. (2012). Phytopathogen effectors subverting host immunity: different foes, similar battleground. Cell Host Microbe **12**:484–495.

Du, Y., Berg, J., Govers, F., and Bouwmeester, K. (2015). Immune activation mediated by the late blight resistance protein R1 requires nuclear localization of R1 and the effector AVR1. New Phytol. **207**:735.

Duan, Z., Xu, H., Ji, X., Zhao, J., Xu, H., Hu, Y., Deng, S., Hu, S., and Liu, X. (2018). Importin α5 negatively regulates importin β1-mediated nuclear import of *Newcastle disease virus* matrix protein and viral replication and pathogenicity in chicken fibroblasts. Virulence **16**:1.

Ellis, J.G., Dodds, P.N., and Lawrence, G.J. (2007). Flax rust resistance gene specificity is based on direct resistance-avirulence protein interactions. Annu. Rev. Phytopathol. **45**:289–306.

Epple, P., Mack, A.A., Morris, V.R., and Dangl, J.L. (2003). Antagonistic control of oxidative stress-induced cell death in *Arabidopsis* by two related, plant-specific zinc finger proteins. Proc. Natl. Acad. Sci. U S A **100**:6831–6836.

Gamir, J., Darwiche, R., Van'T Hof, P., Choudhary, V., Stumpe, M., Schneiter, R., and Mauch, F. (2017). The sterol-binding activity of PATHOGENESIS RELATED PROTEIN 1 reveals the mode of action of an antimicrobial protein. Plant J. **89**:502–509.

Garnica, D.P., Nemri, A., Upadhyaya, N.M., Rathjen, J.P., and Dodds, P.N. (2014). The ins and outs of rust haustoria. PLoS Pathog. **10**:e1004329.

Golovkin, M., and Reddy, A.S. (1998). The plant U1 small nuclear ribonucleoprotein particle 70K protein interacts with two novel serine/arginine-rich proteins. Plant Cell **10**:1637–1647.

Goodin, M.M., Dietzgen, R.G., Schichnes, D., Ruzin, S., and Jackson, A.O. (2010). pGD vectors: versatile tools for the expression of green and red fluorescent protein fusions in agroinfiltrated plant leaves. Plant J. **31**:375–383.

Guo, J., Bai, P., Yang, Q., Liu, F., Wang, X., Huang, L., and Kang, Z. (2013). Wheat zinc finger protein TaLSD1, a negative regulator of programmed cell death, is involved in wheat resistance against stripe rust fungus. Plant Physiol. Biochem. **71**:164–172.

Gupta, D.K., Palma, J.M., and Corpas, F.J. (2015). Reactive Oxygen Species and Oxidative Damage in Plants under Stress (USA: Springer).

Hazel, M., Petra, C., Boevink, M.R., Armstrong, L.P., Sonia, G., Juan, M., Stephen, C.W., Jim, L.B., Paul, R.J., and Birch, M. (2013). An RxLR effector from *Phytophthora infestans* prevents re-localisation of two plant NAC transcription factors from the endoplasmic reticulum to the nucleus. PLoS Pathog. **9**:e1003670.

Hemetsberger, C., Herrberger, C., Zechmann, B., Hillmer, M., and Doehlemann, G. (2012). The *Ustilago maydis* effector Pep1 suppresses plant immunity by inhibition of host peroxidase activity. PLoS Pathog. **8**:e1002684.

Huang, J., Gu, L., Zhang, Y., Yan, T., Kong, G., Kong, L., Guo, B., Qiu, M., Wang, Y., Jing, M., et al. (2017). An oomycete plant pathogen reprograms host pre-mRNA splicing to subvert immunity. Nat. Commun. **8**:2051.

Jacobs, K.A., Collins-Racie, L.A., Colbert, M., Duckett, M., Golden-Fleet, M., Kelleher, K., Kriz, R., LaVallie, E.R., Merberg, D., Spaulding, V., et al. (1997). A genetic selection for isolating cDNAs encoding secreted proteins. Gene **198**:289–296.

Jiang, R.H., and Tyler, B.M. (2012). Mechanisms and evolution of virulence in oomycetes. Annu. Rev. Phytopathol. **50**:295.

Jones, J.D., and Dangl, J.L. (2006). The plant immune system. Nature **444**:323–329.

Kang, Z., Huang, L., and Buchenauer, H. (2002). Ultrastructural changes and localization of lignin and callose in compatible and incompatible interactions between wheat and *Puccinia striiformis*. J. Plant Dis. Protect. **109**:25–37.

Karpiński, S., Szechyńska-Hebda, M., Wituszyńska, W., and Burdiak, P. (2013). Light acclimation, retrograde signalling, cell death and immune defences in plants. Plant Cell Environ. **36**:736–744.

Kay, S., Hahn, S., Marois, E., Hause, G., and Bonas, U. (2007). A bacterial effector acts as a plant transcription factor and induces a cell size regulator. Science **318**:648–651.

Kemen, E., Kemen, A.C., Rafiqi, M., Hempel, U., Mendgen, K., Hahn, M., and Voegele, R.T. (2005). Identification of a protein from rust fungi transferred from haustoria into infected plant cells. Mol. Plant Microbe Interact. **18**:1130–1139.

Lamb, C., and Dixon, R.A. (1997). The oxidative burst in plant disease resistance. Annu. Rev. Plant Biol. **48**:251–275.

Liu, C., Pedersen, C., Schultz-Larsen, T., Aguilar, G.B., Madriz-Ordeñana, K., Hovmøller, M.S., and Thordal-Christensen, H. (2016). The stripe rust fungal effector PEC6 suppresses pattern-triggered immunity in a host species-independent manner and interacts with adenosine kinases. New Phytol. https://doi.org/10.1111/nph.14034.

Lo, P.L., Lanver, D., Schweizer, G., Tanaka, S., Liang, L., Tollot, M., Zuccaro, A., Reissmann, S., and Kahmann, R. (2015). Fungal effectors and plant susceptibility. Annu. Rev. Plant Biol. **66**:513–545.

Mangeon, A., Junqueira, R.M., and Sachettomartins, G. (2010). Functional diversity of the plant glycine-rich proteins superfamily. Plant Signal. Behav. **5**:99–104.

Martínez-Cruz, J., Romero, D., de la Torre, F.N., Fernández-Ortuño, D., Torés, J.A., de Vicente, A., and Pérez-García, A. (2018). The functional characterization of *Podosphaera xanthii* effector candidate genes reveals novel target functions for fungal pathogenicity. Mol. Plant Microbe Interact. **31**:914–931.

Mühlenbock, P., Szechyńska-Hebda, M., Płaszczyca, M., Baudo, M., Mateo, A., Mullineaux, P.M., Parker, J.E., Karpińska, B., and Karpiński, S. (2008). Chloroplast signaling and LESION SIMULATING DISEASE1 regulate crosstalk between light acclimation and immunity in *Arabidopsis*. Plant Cell **20**:2339–2356.

Nishimura, T., Mochizuki, S., Ishii-Minami, N., Fujisawa, Y., Kawahara, Y., Yoshida, Y., Okada, K., Ando, S., Matsumura, H., Terauchi, R., et al. (2016). *Magnaporthe oryzae* glycine-rich secretion protein, Rbf1 critically participates in pathogenicity through the focal formation of the biotrophic interfacial complex. PLoS Pathog. **12**:e1005921.

Nowara, D., Gay, A., Lacomme, C., Shaw, J., Ridout, C., Douchkov, D., Hensel, G., Kumlehn, J., and Schweizer, P. (2012). HIGS: host-induced gene silencing in the obligate biotrophic fungal pathogen *Blumeria graminis*. Plant Cell **22**:3130.

Qi, M.S., Link, T.I., Müller, M., Hirschburger, D., Pudake, R.N., Pedley, K.F., Braun, E., Voegele, R.T., Baum, T.J., and Whitham, S.A. (2016). A small cysteine-rich protein from the Asian soybean rust fungus, *Phakopsora pachyrhizi*, suppresses plant immunity. PLoS Pathog. **12**:e1005827.

Qi, T., Zhu, X.G., Tan, C.L., Liu, P., Guo, J., Kang, Z.S., and Guo, J. (2017). Host-induced gene silencing of an important pathogenicity factor *PsCPK1* in *Puccinia striiformis* f. sp. *tritici* enhances resistance of wheat to stripe rust. Plant Biotechnol. J. **16**:797–807.

Rustérucci, C., Aviv, D.H., Holt, B.F., Dangl, J.L., and Parker, J.E. (2001). The disease resistance signaling components *EDS1* and *PAD4* are essential regulators of the cell death pathway controlled by *LSD1* in *Arabidopsis*. Plant Cell **13**:2211–2224.

Salcedo, A., Rutter, W., Wang, S., Akhunova, A., Bolus, S., Chao, S., Anderson, N., De Soto, M.F., Rouse, M., Szabo, L., et al. (2017). Variation in the *AvrSr35* gene determines *Sr35* resistance against wheat stem rust race Ug99. Science **358**:1604–1606.

Sarris, P.F., Duxbury, Z., UnHuh, S., Ma, Y., Segonzac, C., Sklenar, J., Derbyshire, P., Cevik, V., Rallapalli, G., and Saucet, S.B. (2015). A plant immune receptor detects pathogen effectors that target WRKY transcription factors. Cell **161**:1089–1100.

Tan, Y., Li, M.J., Yang, Y.L., Sun, X., Wang, N., Liang, B.W., and Ma, F.W. (2017). Overexpression of *MpCYS4*, a phytocystatin gene from *Malus prunifolia* (Willd.) Borkh., enhances stomatal closure to confer drought tolerance in transgenic *Arabidopsis* and Apple. Front. Plant Sci. **8**:33.

Tang, C., Xu, Q., Zhao, M., Wang, X., and Kang, Z. (2018). Understanding the lifestyles and pathogenicity mechanisms of obligate biotrophic fungi in wheat: the emerging genomics era. Crop J. **6**:60–67.

Thomma, B.P., Nürnberger, T., and Joosten, M.H. (2011). Of PAMPs and effectors: the blurred PTI-ETI dichotomy. Plant Cell **23**:4–15.

Torto-Alalibo, T., Collmer, C.W., Gwinn-Giglio, M., Lindeberg, M., Meng, S., Chibucos, M.C., Tseng, T.T., Lomax, J., Biehl, B.,

Ireland, A., et al. (2010). Unifying themes in microbial associations with animal and plant hosts described using the gene ontology. Microbiol. Mol. Biol. Rev. **74**:479–503.

Torres, M.A. (2010). ROS in biotic interactions. Physiol. Plantarum **138**:414.

Upadhyaya, N.M., Mago, R., Staskawicz, B.J., Ayliffe, M.A., Ellis, J.G., and Dodds, P.N. (2014). A bacterial type III secretion assay for delivery of fungal effector proteins into wheat. Mol. Plant Microbe Interact. **27**:255–264.

Wang, W., Ye, R., Xin, Y., Fang, X., Li, C., Shi, H., Zhou, X., and Qi, Y. (2011). An importin β protein negatively regulates microRNA activity in *Arabidopsis*. Plant Cell **23**:3565–3576.

Wang, X., Wang, X., Feng, H., Tang, C., Bai, P., Wei, G., Huang, L., and Kang, Z.S. (2012). *TaMCA4*, a novel wheat metacaspase gene functions in programmed cell death induced by the fungal pathogen *Puccinia striiformis* f. sp. *tritici*. Mol. Plant Microbe Interact. **25**:755–764.

Wang, X., Yang, B., Li, K., Kang, Z., Cantu, D., and Dubcovsky, J. (2016). A conserved *Puccinia striiformis* protein interacts with wheat NPR1 and reduces induction of pathogenesis-related genes in response to pathogens. Mol. Plant Microbe Interact. **29**:977–989.

Xu, C., and He, C. (2007). The rice *OsLOL2* gene encodes a zinc finger protein involved in rice growth and disease resistance. Mol. Genet. Genomics **278**:85–94.

Yang, G., Yang, G., Tang, L., Gong, Y., Xie, J., Fu, Y., Jiang, D., Li, G., Collinge, D.B., Chen, W., et al. (2018). A cerato-platanin protein SsCP1 targets plant PR1 and contributes to virulence of *Sclerotinia sclerotiorum*. New Phytol. **217**:739–755.

Ye, W., and Ma, W. (2016). Filamentous pathogen effectors interfering with small RNA silencing in plant hosts. Curr. Opin. Microbiol. **32**:1–6.

Yeh, S., Lin, C., Wu, F., and Wang, A. (2011). Analysis of the expression of *BohLOL1*, which encodes an LSD1-like zinc finger protein in *Bambusa oldhamii*. Planta **234**:1179–1189.

Zhang, S., and Xu, J. (2014). Effectors and effector delivery in *Magnaporthe oryzae*. PLoS Pathog. **10**:e1003826.

Zhang, M., Li, Q., Liu, T., Liu, L., Shen, D., Zhu, Y., Liu, P., Zhou, J.M., and Dou, D. (2015). Two cytoplasmic effectors of *Phytophthora sojae* regulate plant cell death via interactions with plant catalases. Plant Physiol. **167**:164–175.

Zheng, W., Huang, L., Huang, J., Wang, X., Chen, X., Zhao, J., Guo, J., Zhuang, H., Qiu, C., Liu, J., et al. (2013). High genome heterozygosity and endemic genetic recombination in the wheat stripe rust fungus. Nat. Commun. **4**:2673.

Zhu, X.G., Qi, T., Yang, Q., He, F.X., Tan, C.L., Ma, W., Voegele, R.T., Kang, Z.S., and Guo, J. (2017). Host-induced gene silencing of the MAPKK gene *PsFUZ7* confers stable resistance to wheat stripe rust. Plant Physiol. **175**:1853–1863.